Normal and Variant Pelvic Anatomy on MRI

Ashish P. Wasnik, MBBS, MD[a], Michael B. Mazza, MD[a], Peter S. Liu, MD[a,b,*]

KEYWORDS

• Pelvic anatomy • MRI • Variant anatomy • Pelvic viscera

Because of its superior tissue contrast, native multiplanar capabilities, and nonionizing technique, magnetic resonance imaging (MRI) is well suited for evaluation of the pelvis. Although ultrasound is frequently indicated for the primary evaluation of suspected genitourinary pathology in both men and women, it can be limited by body habitus, depth of acoustic penetration, and ability to discriminate between specific tissue types.[1,2] Knowledge of normal pelvic anatomy on MRI is critical for proper interpretation, in particular the standard visceral organ appearances, commonly encountered variants, and pathology mimics. Because most pelvic MRI studies are targeted toward an organ or area of interest, this article discusses the protocol strategies and relevant anatomy in a segmented/organ-specific manner, using gender as a broad split given the substantial variance in relevant organs.

FEMALE PELVIS

Technical Considerations

At the authors' institution, the female pelvis protocol is performed for suspected ovarian, uterine, vaginal, or bladder pathology; a separate protocol is used for high-resolution imaging of the female urethra. Studies are performed using a phased-array surface coil and intramuscular injection of an antiperistaltic agent to suppress bowel motion, which improves visualization of the adnexal and peritoneal surfaces.[2,3]

The basic female pelvis protocol begins with a coronal T2-weighted single-shot echo-train spin-echo technique (such as single-shot fast spin-echo [SSFSE] or half-Fourier acquisition single-shot turbo spin-echo [HASTE]), with wide field of view (FOV) to include portions of the kidneys, due to the coexistent risk of renal anomalies in the setting of suspected genitourinary developmental disorders.[4] Subsequently, a sagittal T2-weighted fast spin-echo sequence is used to delineate the uterine lie, demonstrate the zonal anatomy of the uterus, and provide improved anatomic landmarks for subsequent uterine image planning (**Fig. 1**). Both short-axis and long-axis T2-weighted fast spin-echo images are then obtained to provide redundant detail of the uterine zonal anatomy and optimize evaluation of the external uterine contour (**Figs. 2** and **3**). T1-weighted imaging is initially accomplished using a breath-hold spoiled gradient-echo sequence in which both in-phase and opposed-phase echoes are recorded (**Figs. 4–6**). Subsequently, T1-weighted imaging using chemical fat suppression is performed, which aids in the differentiation of lipid and hemorrhagic/proteinaceous pathologies on T1-weighted imaging. Additional postcontrast images are obtained using the same sequence (see **Figs. 4–6**). If a patient is evaluated for fibroid disease and potential uterine artery embolization, a dynamic oblique coronal magnetic resonance angiography sequence augments the normal precontrast and postcontrast axial imaging, which

[a] Department of Radiology, University of Michigan Health System, 1500 East Medical Center Drive, Ann Arbor, MI 48109-0030, USA
[b] Department of Vascular Surgery, University of Michigan Health System, 1500 East Medical Center Drive, Ann Arbor, MI 48109-0030, USA
* Corresponding author. Department of Radiology, University of Michigan Health System, 1500 East Medical Center Drive, Ann Arbor, MI 48109-0030.
E-mail address: peterliu@umich.edu

Magn Reson Imaging Clin N Am 19 (2011) 547–566
doi:10.1016/j.mric.2011.05.001

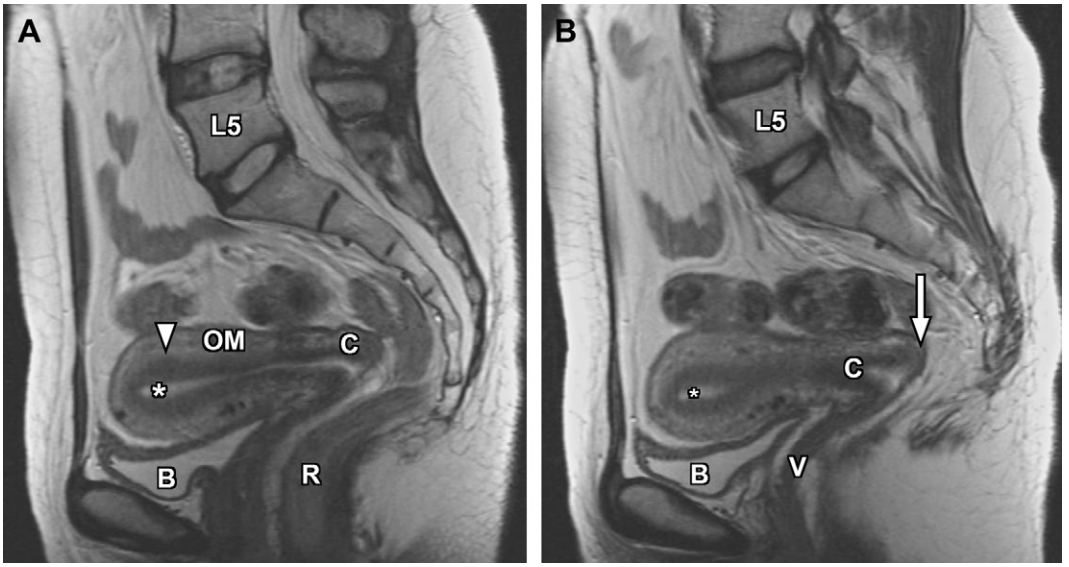

Fig. 1. Sagittal T2-weighted images of the female pelvis in midline (*A*) and paramidline (*B*) locations. The zonal anatomy of the uterus is well demonstrated on T2-weighted images, with high signal intensity in the endometrium (*asterisk*) and characteristic low signal intensity of the junctional zone (*arrowhead*). Outer myometrium demonstrates intermediate signal intensity between the two other uterine layers. The cervix is well seen in longitudinal dimension, noting contiguity of the dark fibromuscular stroma with the uterine junctional zone. The posterior fornix (*arrow*) is formed from the posterior reflection/interface of the exocervix and the vagina. B, bladder; C, cervix; L5, L5 vertebral level; OM, outer myometrium; R, rectum; V, vagina.

aids in prediction of anomalous ovarian arterial supply to uterine fibroids.[5]

For specific evaluation of the female urethra, a high-resolution protocol is employed. Most patients are examined using an endoluminal coil placed in the vagina to improve signal-to-noise ratio at higher spatial resolutions.[6] The protocol begins with axial, sagittal, and coronal T2-weighted fast spin-echo imaging sequences using a focused small FOV (**Fig. 7**A, C). Subsequently, precontrast axial T1-weighted spin-echo imaging is performed with a similar small FOV. Chemical fat suppression is then added to this T1-weighted sequence, which is repeated for both precontrast and postcontrast imaging (see **Fig. 7**B). In patients who are unable to tolerate local coil placement in the vagina, the female pelvis protocol with phased-array surface coil can be substituted, focusing mostly on the perineum rather than the uterus; in this setting, long-axis and short-axis T2-weighted imaging is converted to traditional axial and coronal planes.

Anatomic Considerations and MRI Features

Magnetic resonance has a significant role in evaluation of the pelvic abnormalities, including uterine, ovarian, cervical, adnexal, and congenital abnormalities. A better understanding of anatomy remains crucial in the evaluation of congenital abnormalities as well as in characterization of a lesion and its extent.

Uterus and cervix

The uterus can be divided into 3 segments: fundus, body, and cervix. The uterine body or corpus consists of 3 layers; from central to peripheral, these include the endometrium, junctional zone, and myometrium.

The endometrium is the central most portion of the uterus, with a varying thickness that changes during the menstrual cycle—it is wider during the secretory phase than during follicular phase or menstruation.[7–9] The normal endometrial thickness varies depending on age, with thickness of less than 10 mm considered normal in reproductive age women, whereas a thickness of less than 5 mm is considered normal in postmenopausal women.[7] Women on hormonal replacement therapy can have endometrial thickness ranging from 5 to 8 mm. The endometrium is typically high signal on T2-weighted images (see **Figs. 1–3**), although not as high signal as simple fluid in the adjacent urinary bladder and homogeneous low signal intensity on precontrast T1-weighted images (see **Figs. 4–7**).

The junctional zone represents the innermost layer of the myometrium and demonstrates a characteristic low signal intensity relative to myometrium

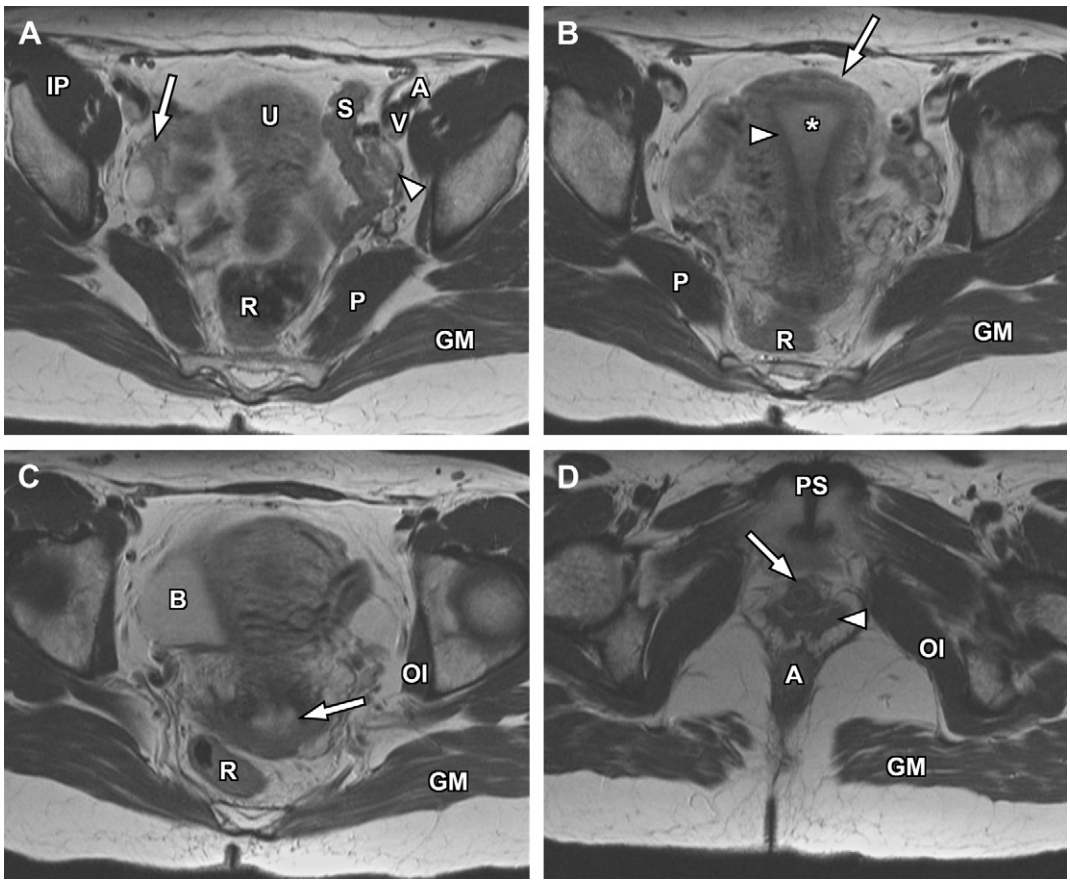

Fig. 2. (*A*) Oblique T2-weighted long-axis image of the pelvis, superior cut through uterus. The long-axis of the uterus is partially visualized on this image. Several pelvic structures are well delineated, including right ovary (*arrow*) and left ovary (*arrowhead*). (*B*) Oblique T2-weighted long-axis image of the pelvis, middle cut through uterus. This long-axis view of the uterus shows the external uterine contour (*arrow*) in a single image, in this case slightly convex outward. The zonal anatomy is well seen on this central uterine image, including endometrium (*asterisk*) and junctional zone (*arrowhead*). (*C*) Oblique T2-weighted long-axis image of the pelvis, inferior cut through uterus. The uterus is only partially visualized at this level. The cervix and upper vagina, however, are now in plane (exocervix [*arrow*]). (*D*) Oblique T2-weighted long-axis image of the pelvis toward the perineum. At this level, the urethra (*arrow*) and vagina (*arrowhead*) are well seen. The anal canal is also visible. A (*A*), external iliac artery; A (*C*), anal canal; B, bladder; GM, gluteus maximus muscle; IP, iliopsoas muscle; OI, obturator internus muscle; PS, pubic symphysis; P, piriformis muscle; R, rectum; S, sigmoid colon; V, external iliac vein.

on T2-weighted images (see **Figs. 1–3**), likely from a multifactorial basis.[10] These described factors include the presence of compact smooth muscles, decreased water content of the cells versus the outer myometrium, and increased number and size of nuclei compared with outer myometrium.[10–12] The normal junctional zone can vary in size, but a thickness greater than 12 mm is considered abnormal.[10,13,14] The junctional zone can be poorly demarcated in postmenopausal women.

The outer myometrium is structurally different than the junctional zone, with increased cellular free water and decreased cell packing/density. This results in intermediate increased signal intensity on T2-weighted images (see **Figs. 1–3**), substantially higher than the junctional zone but generally lower than the hyperintense endometrium. The entire uterus is of intermediate signal intensity on T1-weighted images relative to muscle with no clear demarcation of different zones (see **Figs. 4–7**).[15]

The cervix is separated from the uterine body by the internal os. Three discrete cervical zones can be identified on high-resolution T2-weighted images. The central hyperintense zone is formed by the endocervical canal with its mucosa, secretions, and plica palmatae/longitudinal folds. Peripheral to this, there is a middle layer, which represents the inner fibromuscular stroma, characterized by hypointense features on T2-weighted imaging due to

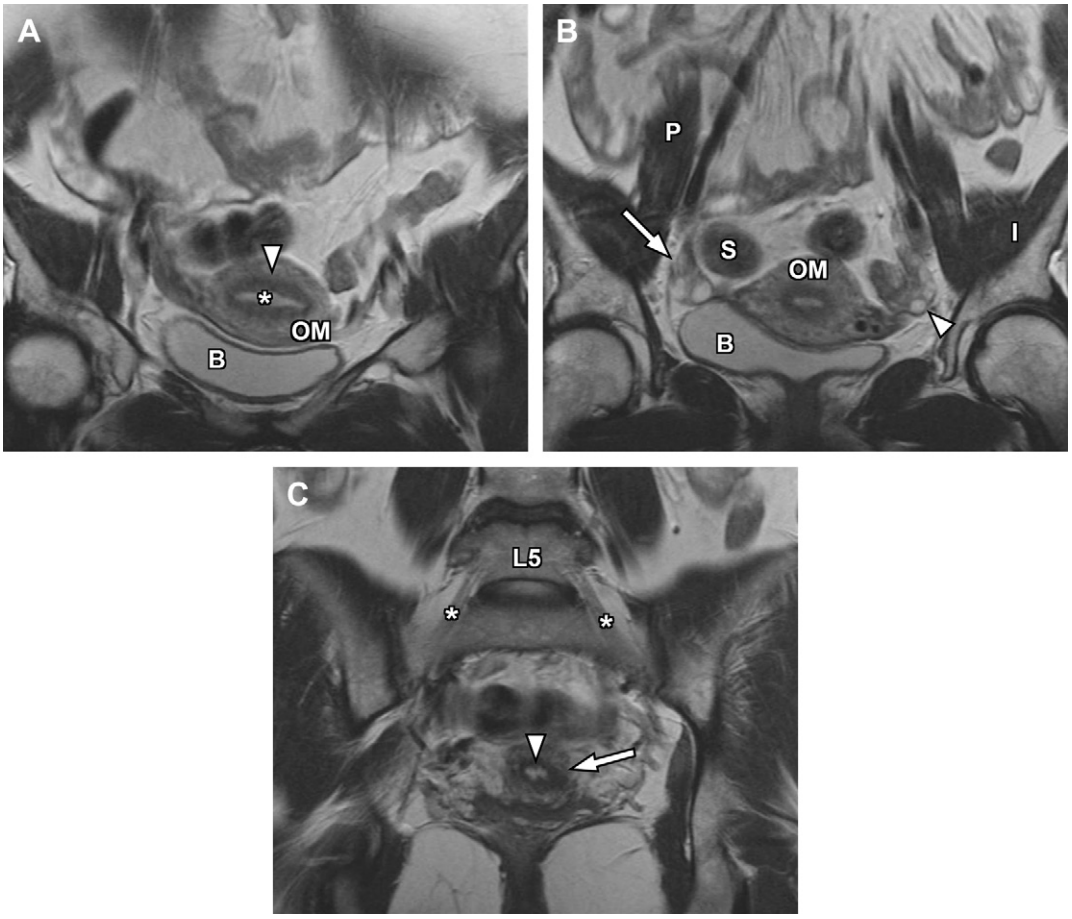

Fig. 3. (*A*) Oblique T2-weighted short-axis image of the pelvis, anterior cut through the uterus. Zonal anatomy is well demonstrated on short-axis imaging, including endometrium (*asterisk*), junctional zone (*arrowhead*), and outer myometrium. (*B*) Oblique T2-weighted short-axis image of the pelvis, central cut through the uterus. Zonal anatomy is gain well seen though uterine size is decreasing toward the lower uterine segment; only the outer myometrium is marked. Both ovaries are demonstrated (right ovary [*arrow*]; left ovary [*arrowhead*]). (*C*) Oblique T2-weighted short-axis image of the pelvis, posterior cut through the uterus. Cervix is now seen (*arrow*). Longitudinal fold of the cervical folds/plicae palmatae is well seen in cross section (*arrowhead*). Exiting nerve L5 roots (*asterisk*) are well seen given slight obliquity of image. B, bladder; I, iliacus muscle; L5, L5 vertebral body; OM, outer myometrium; P, psoas muscle; S, sigmoid colon.

fibrous stroma and dense smooth muscle. The peripheral outer layer demonstrates a more modest signal intensity, often low-intermediate signal on T2-weighted images, corresponding to the outer fibromuscular stroma. The inner fibromuscular stroma/middle layer is frequently contiguous with the junctional zone in many women, whereas the outermost layer may be contiguous with the outer uterine myometrium.[16–18] On T1-weighted images, there is no apparent distinction between different layers of the cervix; however, after the administration of intravenous gadolinium contrast, the endocervical mucosa enhances more rapidly than the fibromuscular stroma.[17,19]

Congenital uterine anomalies comprise a wide spectrum of variant anatomy. The true prevalence of uterine anomalies has been difficult to assess, with varying reported rates between 0.16% and 10%, often confounded by selection bias or variance in classification schemes.[4] Abnormal uterine configurations are typically related to developmental problems of the paramesonephric or müllerian ducts in the first trimester fetus. The paired müllerian ducts join together to form the uterus and upper vagina. After fusion, a midline septum is resorbed as the uterus assumes its normal configuration. Conceptually, müllerian fusion abnormalities can be broadly characterized into 3 categories: agenesis/hypoplasia, defects in vertical fusion, and defects in lateral fusion.[18] The modern and widely used classification scheme developed by the American Fertility Society

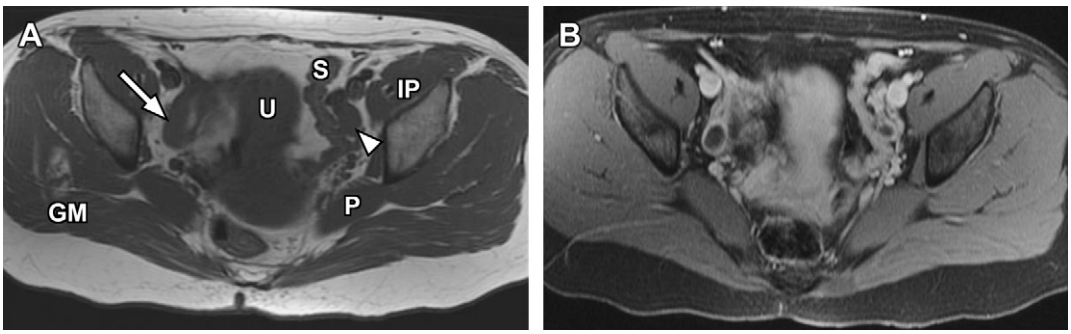

Fig. 4. Axial T1-weighted image in upper pelvis, precontrast (*A*) and fat-suppressed postcontrast (*B*). Zonal anatomy of the uterus (U) is not well seen on T1-weighted images. The follicular architecture of the ovaries (right ovary [*arrow*], left ovary [*arrowhead*]) is also not as well seen as T2-weighted images, although some follicles are more easily seen on postcontrast imaging due to lack of internal enhancement. Muscular architecture is well depicted, including iliopsoas muscle (IP), gluteus maximus muscle (GM), and piriformis muscle (P). S, sigmoid colon.

divides congenital anomalies into 7 discrete classes; associated vaginal or cervical abnormalities are reported as subsets of the major classes.[20] Although many cases can be placed into a single category, it is possible for individual cases to overlap classes or fall along a spectrum of classical disease.

Disorders of agenesis and hypoplasia form the basis for class I anomalies, usually resulting from failure of müllerian duct development before potential fusion. Class I anomalies account for approximately 5% to 10% of all müllerian fusion anomalies.[4] Classically, complete bilateral agenesis of the entire uterus and upper vagina is termed, *Mayer-Rokitansky-Küster-Hauser syndrome* (Fig. 8). In 10% of such cases, isolated vaginal agenesis may be present with a rudimentary or obstructed uterine remnant in place.[4,18] Clinically, these patients present with normal female phenotype but demonstrate primary amenorrhea. MRI demonstrates normal female gonads/ovaries but agenesis of the uterus and upper vagina (see Fig. 8).

Class II anomalies result from failure of a single müllerian duct to develop normally, causing an asymmetry of the mature uterus called a unicornuate uterus (Fig. 9). This accounts for approximately 20% of all müllerian fusion anomalies.[4] There are 3 general subtypes, occurring in approximately similar frequencies, including an isolated single horn, a rudimentary second horn without functional endometrium, and a rudimentary second horn containing an endometrial segment.[18] In the latter situation, the endometrial tissue/cavity may or may not communicate with the endometrial space in the normal horn on the contralateral side—noncommunication is more common than communication by approximately a 2:1 ratio. Unicornuate uterus can be clinically occult, but the presence of a noncommunicating rudimentary

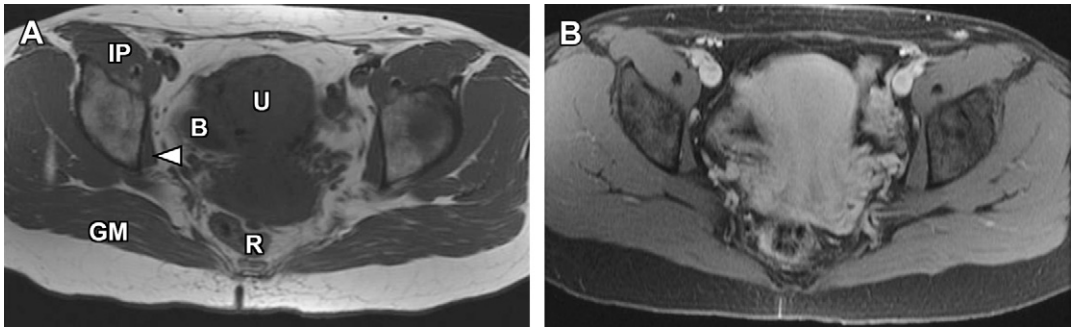

Fig. 5. Axial T1-weighted image in mid pelvis, precontrast (*A*) and fat-suppressed postcontrast (*B*). The uterus remains relatively homogeneous is signal intensity, with only subtle differential signal on postcontrast imaging to suggest zonal anatomy. Bladder is partially visualized, with low signal intensity expected for normal urine. Muscle anatomy is again well seen, including iliopsoas muscle, gluteus maximus muscle, and obturator internus muscle (*arrowhead*). B, bladder; GM, gluteus maximum; IP, iliopsoas muscle; R, rectum; U, uterus.

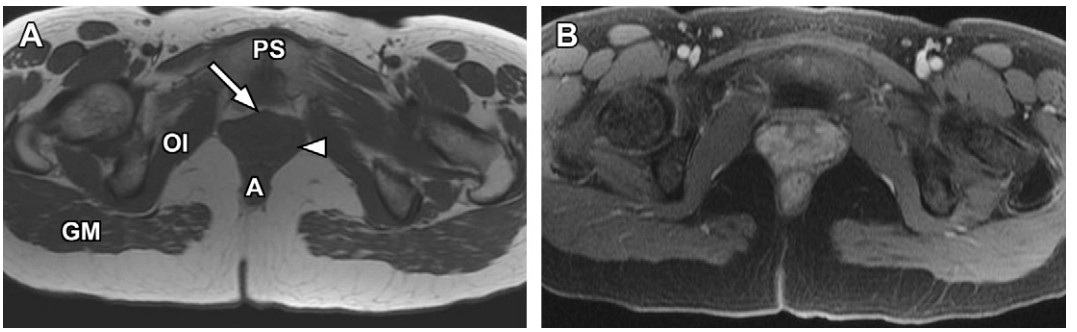

Fig. 6. Axial T1-weighted image in lower pelvis, precontrast (*A*) and fat-suppressed postcontrast (*B*). The structural anatomy seen at this level on T2-weighed images is more difficult to appreciate, particularly on precontrast T1-weighted images. Urethra (*arrow*) and vagina (*arrowhead*) are present anteriorly, whereas anal canal is present posteriorly. A, anal canal; GM, gluteus maximus muscle; OI, obturator Internus muscle; PS, pubic symphysis.

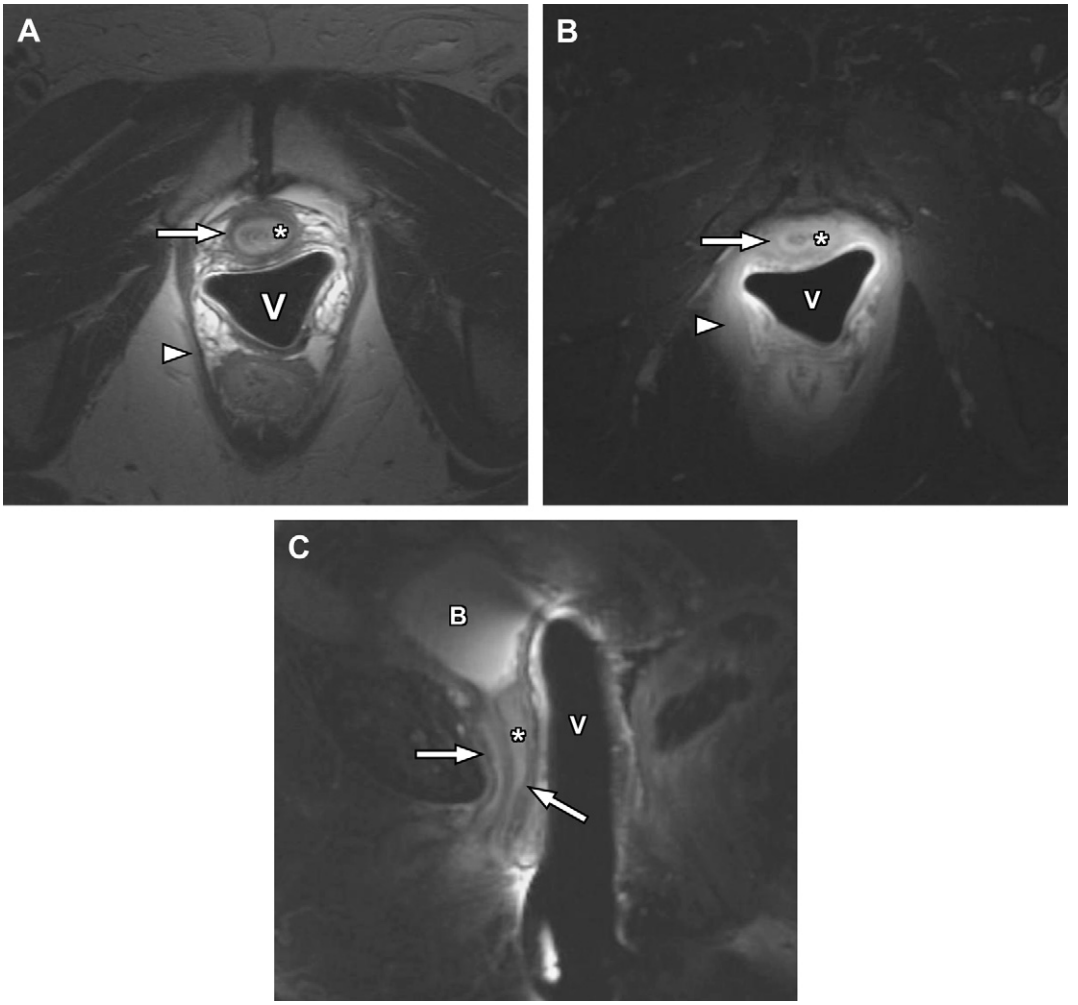

Fig. 7. Small FOV urethral imaging, including axial T2 weighted (*A*), axial fat-suppressed postcontrast T1 weighted (*B*), and sagittal T2 weighted (*C*). The concentric layers of the female urethra are well depicted, including high signal intensity submucosa (*asterisk*) and low signal intensity outer muscular layer (*arrows*). Vagina is distended with air due to indwelling receiver coil. Levator ani muscle group (*arrowhead*). B, bladder; V, vagina.

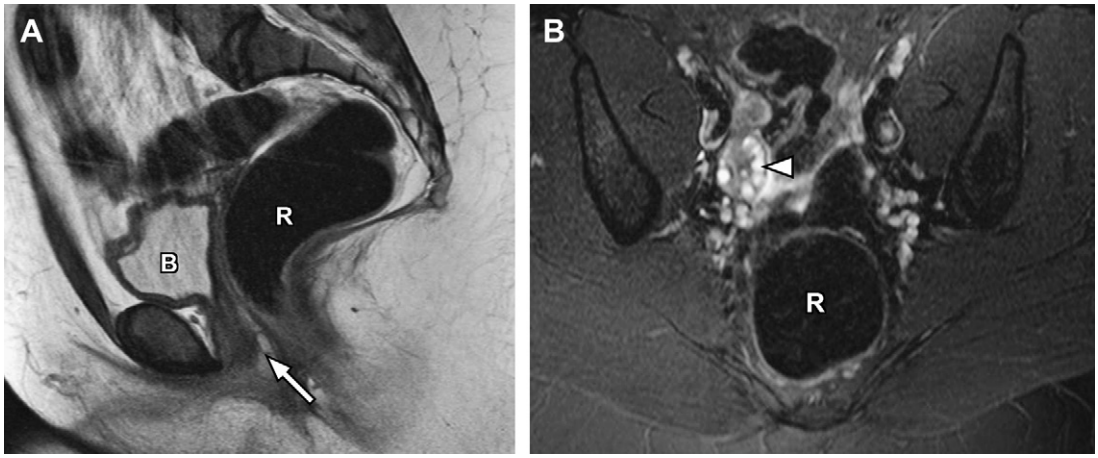

Fig. 8. Mayer-Rokitansky-Küster-Hauser syndrome. Sagittal T2-weighted (*A*) and axial fat-suppressed T2-weighted (*B*) images demonstrate urinary bladder (B) and rectum (R). There is no uterus, however, seen in the midline. Diminutive outer vagina/introitus (*arrow*) was seen on physical examination. Higher in the pelvis, normal ovaries were demonstrated (right ovary [*arrowhead*]), confirming female gonads.

horn is often associated with dysmenorrhea and hematometra. Surgery is often indicated for rudimentary horns that have associated endometrial tissue, regardless of whether or not they communicate, due to potential pregnancy issues and symptomatic relief, respectively. On MRI, unicornuate uterus has a curvilinear shape resembling a banana with normal zonal differentiation in the mature horn. The presence of a rudimentary horn should be noted, though the zonal anatomy may be absent if there is no functional endometrial tissue.[4]

Class III and IV anomalies represent fusion defects between the paired müllerian ducts, including incomplete midline fusion (class III, bicornuate uterus) and near total failure of midline fusion (class IV, uterus didelphys). Together, these account for approximately 15% of all müllerian fusion anomalies, with bicornuate uterus more common than uterus didelphys by approximately a 2:1 ratio.[4] A bicornuate uterus has cephalad separation of the uterine horns, with some midline fusion seen along the caudal margin of the uterine body or lower uterine segment (**Fig. 10**). Duplication of the cervix is variable in bicornuate uterus, offering both single (unicollis) and double (bicollis) cervix subtypes. Uterus didelphys has 2 widely splayed uterine horns with almost no observed midline fusion (**Fig. 11**) extending through the

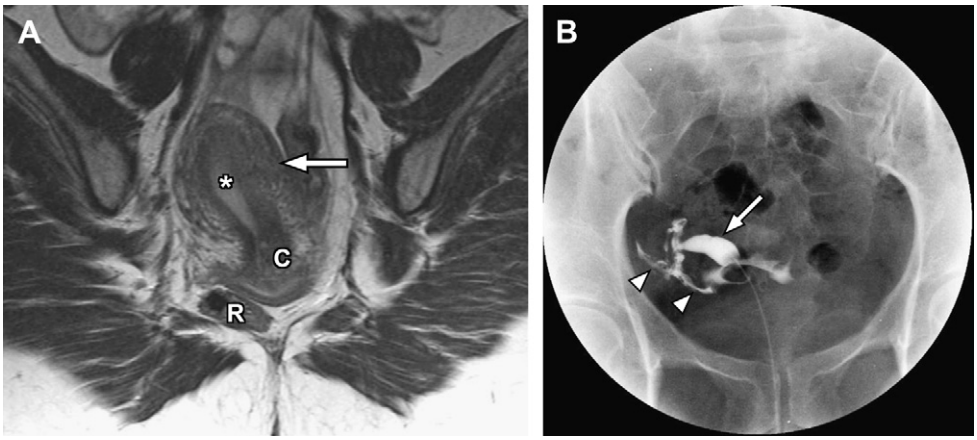

Fig. 9. Unicornuate uterus. Oblique T2-weighted long-axis image (*A*) and fluoroscopic spot image from hysterosalpingography (*B*). Rather than assuming a normal triangular shape, the uterus (*arrow*) has a curvilinear shape, similar to a banana. Normal zonal anatomy is seen, including hyperintense endometrium (*asterisk*). Cervix (C) and rectum (R) are both demonstrated on MRI image. Unicornuate uterine configuration is confirmed on hysterosalpingogram with free spill of contrast through the single horn and tube (*arrowheads*).

lower uterine segment; duplicated cervices are present.[18] On MRI, both entities are characterized by a split uterine horns that demonstrate zonal uterine anatomy. The key feature is a deep concavity of the expected uterine fundus, with a cleft of at least 1 cm diagnostic. Because of the multiplanar nature of MRI, this determination is straightforward on oblique imaging obtained along the uterine long axis. Once the fundal cleft is established, attention is turned to degree of midline fusion, either partial or near absent, to differentiate between bicornuate uterus and uterus didelphys. Presence of 2 cervices cannot be relied on for differentiation because it is present in both bicornuate uterus bicollis subtype and uterus didelphys.

Accounting for approximately 55% of all müllerian fusion anomalies, the septate uterus (class V) is the most common uterine anomaly (**Fig. 12**).[4] The developmental defect associated with septate uterus occurs after midline fusion, during the septal resorption phase, including both partial and total failure of septal resorption. The resultant longitudinal septum extends caudally from the uterine fundus and is termed complete if it extends to the external cervical os; approximately 25% of patients have septal extension into the upper vagina.[4] Because of differences in treatment for patients with septate uterus versus those with bicornuate or didelphys configurations, differentiating these entities is critical. On MRI, a septate uterus shows a normal configuration, either convex outward, flat, or minimally concave with a fundal cleft/depth of less than 1 cm on long-axis imaging. The signal intensity of the septum is important, because muscular septa demonstrate similar characteristics to background myometrium, whereas fibrous septa are generally thinner with dark signal on T2-weighted images.

The final 2 classes of müllerian fusion anomalies are unique. Class VI refers to an arcuate configuration, which some authors consider a normal variant rather than a müllerian fusion anomaly. On MRI, an arcuate configuration has a broad-based shallow bulge of the inner fundal myometrial contour, with a normal outer fundal contour. Class VII is a specific uterine configuration related to in utero exposure to diethylstilbestrol (DES), a synthetic estrogen that was thought to decrease the rate of pregnancy loss in patients with prior spontaneous abortions or premature deliveries. In utero DES exposure was shown to interfere with embryologic genital tract development, causing resultant structural abnormalities in the term fetus, and was discontinued in 1971. Classically, the anomaly linked to prior DES exposure was a hypoplastic uterus with a T-shaped configuration of the endometrial cavity. Several other anomalies of the cervix and fallopian tubes have also been reported.

Both physiologic events and acquired defects can alter the apparent uterine anatomy. Functional myometrial contractions occur in the junctional zone and can distort the endometrium, but generally do not affect the myometrium (**Fig. 13**).[21–23] Although commonly seen in gravid uterus, they can be present in the nongravid uterus as well.

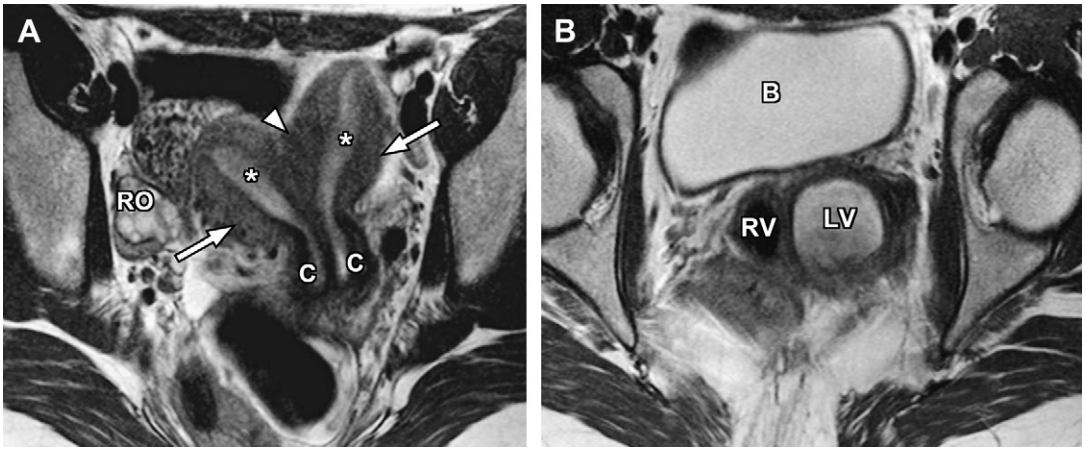

Fig. 10. Bicornuate bicollis uterus. Oblique T2-weighted long-axis images (*A* and *B*) through the uterus and lower pelvis, demonstrating 2 uterine horns (*arrows*) with deep fundal cleft (*arrowhead*) but some maintained midline fusion. Normal zonal anatomy is present in both horns (endometrium [*asterisk*]). Duplicated cervices are present, and lower images demonstrate duplication of the upper vagina with tampon in right hemivagina and obstructed left hemivagina. B, bladder; C, cervices; LV, left hemivagina; RO, right ovary; RV, right hemivagina.

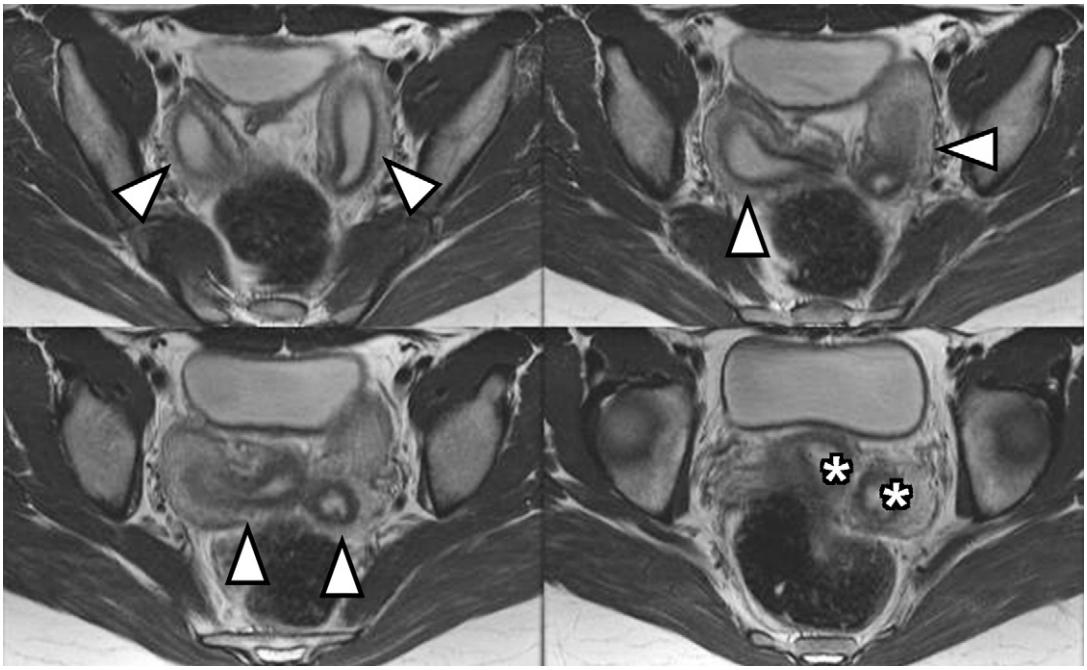

Fig. 11. Uterus didelphys. Several axial T2-weighted images demonstrate widely splayed uterine horns (*arrowheads*) with no midline fusion. Duplicated cervices are also present (*asterisk*).

The rounded nature of a contraction can mimic a fibroid or adenomyosis.[22] Contractions should resolve or change, however, during the course of the MRI study. After cesarean section, a small scar/defect is present along the lower uterine segment (**Fig. 14**). During the early postpartum period, this scar may demonstrate high signal on both T1-weighted and T2-weighted images due to subacute hematoma in the uterine incision.[24]

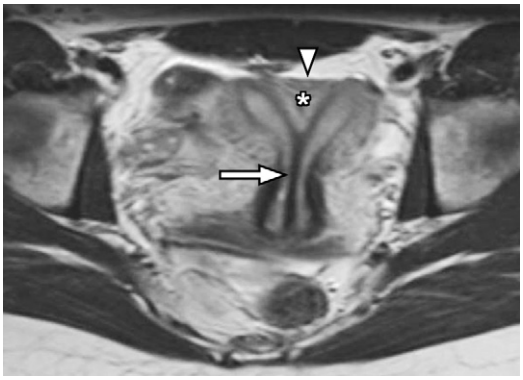

Fig. 12. Septate uterus. Oblique T2-weighted long-axis image demonstrates flat outer uterine contour (*arrowhead*) with mixed muscular (*asterisk*) and fibrous (*arrow*) septum coursing through the midline, including extension into the cervix.

Vagina

The vagina is a fibromuscular tube measuring approximately 7 to 9 cm in length, extending from the vulva inferiorly to the cervix superiorly and lying between the bladder and rectum. It is attached to the levator ani at the level of the urogenital diaphragm. It is lined by estrogen-sensitive stratified squamous epithelium. The layers of the vagina are the inner mucosal layer, middle submucosal/muscular layer, and outer adventitial layer consisting of a vaginal venous plexus. For descriptive purposes the vagina is divided into thirds, with the lower third defined as below the level of the bladder base with the urethra seen immediately anterior to it. The middle third corresponds to the level of the bladder base, whereas the upper third corresponds to the lateral vaginal fornices. The arterial supply is from a network of vessels formed by anastomosis between the vaginal and uterine branches of the internal iliac artery, with the mid and lower thirds of the vagina supplied by the middle rectal artery and internal pudendal arteries. Venous drainage is via the uterine and vaginal venous plexuses into the internal iliac veins.

The vulva is comprised of the mons pubis, the labia majora and minora, the clitoris, the vestibular bulb, vestibular glands, and the vestibule of the vagina. Blood supply is from branches of the external and internal pudendal arteries.

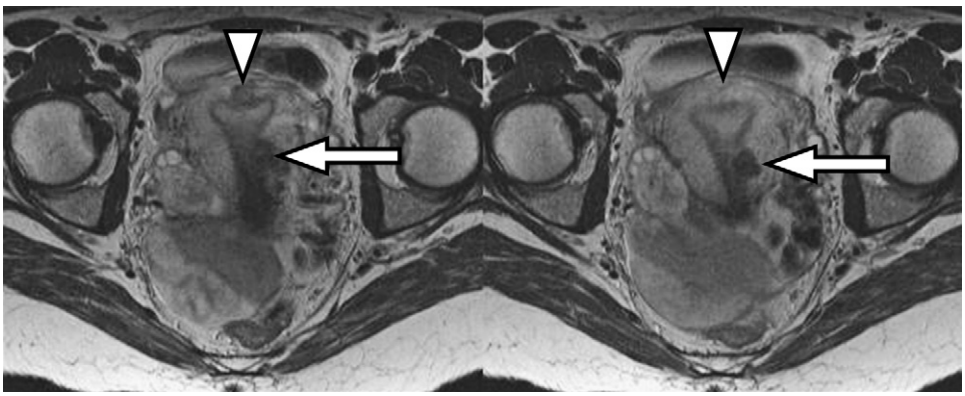

Fig. 13. Functional myometrial contraction. Oblique T2-weighted long-axis images taken several minutes apart demonstrate a focal low signal intensity near the uterine fundus (*arrowhead*), which is present on the first image (*left*) but not seen on the repeat image several minutes later (*right*), compatible with a myometrial contraction. Note slight indentation on the endometrial surface associated with this contraction. Fibroid (*arrow*).

The vaginal layers are best seen on T2-weighted images.[25] The vaginal mucosa with intraluminal fluid demonstrates high signal intensity on T2-weighted images and low signal intensity on T1-weighted images. The submucosal and the muscularis layer are low signal intensity on both T1-weighted and T2-weighted imaging. The adventitial layer demonstrates high signal intensity on T2-weighted images due to presence of well-developed venous plexus that has slow flow.[18,25–27] After intravenous gadolinium administration, the vaginal mucosa enhances. Signal characteristics of the vaginal wall and thickness of the mucosal layer vary depending on the phase of the menstrual cycle, paralleling estrogen levels.[25,28] The vulva shows low to intermediate signal intensity on T1-weighted imaging and slightly higher signal intensity on T2-weighted imaging.[28]

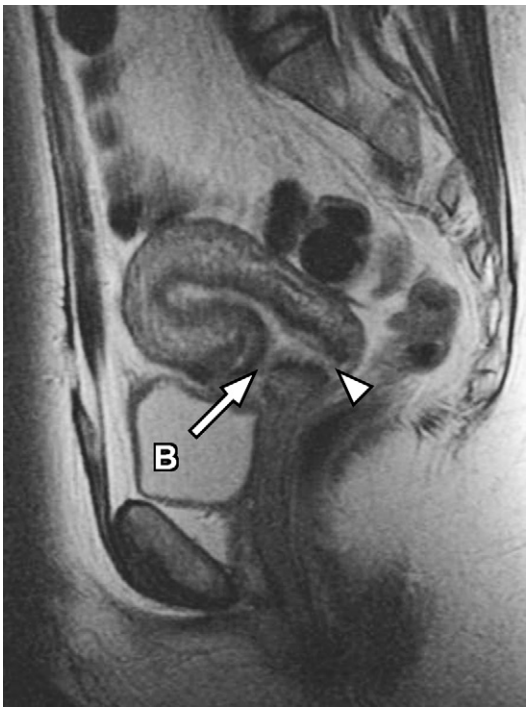

Fig. 14. Cesarean section scar. Sagittal T2-weighted image demonstrates anterior linear defect in the lower uterine segment (*arrow*) compatible with cesarean section scar. Normal cervix is noted more posteriorly (*arrowhead*), in line with the longitudinal axis of the uterus. B, bladder.

Female urethra

Female urethra is thin-walled tubular muscular channel, measuring approximately 40 mm in length, coursing anteroinferiorly from internal urethral meatus located at bladder trigone and terminating in an external urethral meatus anterior to the vagina. Tiny glands in the periurethral tissues (Skene glands) secrete mucus during sexual intercourse. The lower two-thirds of the urethra is lined by stratified squamous epithelium and the proximal one-third is lined by transitional epithelium. The urethra has 3 layers, including an inner mucosal layer, a vascular submucosal layer, and an outer muscular layer. Urethropelvic ligaments provide structural support to the urethra.

T2-weighted sequence using endoluminal coils is best suited for demonstration the urethral zonal anatomy.[26,29,30] The zonal anatomy is almost similar to the vaginal layers on T2-weighted images, with low signal intensity inner mucosal layer, a high signal intensity vascular submucosal layer and low signal intensity outer muscular layer, giving a target appearance on transverse images (see **Fig. 7**A).[31,32] The intraluminal fluid or urine is high signal intensity on T2-weighted images.[18]

The zonal anatomy is indistinct on noncontrast T1-weighted images with increased enhancement of the submucosal layer on postgadolinium T1-weighted images (see Fig. 7B). In postmenopausal women, the zonal anatomy may be poorly defined. In patients with stress incontinence, atrophy of the outer muscular layer can be noted.[33]

Ovaries

The ovaries are located within a depression in pelvic sidewall, called the ovarian fossa. The location of the ovaries may vary based on multiparity, size of uterus, and bladder distension. The ovaries are held in position by several ovarian suspensory ligaments.[34] Arterial vascular supply to the ovaries is provided by an ovarian artery, directly branching from the abdominal aorta below the origin of renal arteries. Small anastomoses exist with channels originating from the uterine arteries. The venous drainage occurs through the gonadal vein, with the right gonadal vein draining directly into the inferior vena cava just below the right renal vein insertion and the left gonadal vein draining into the left renal vein.

In premenopausal women, T2-weighted images reveal zonal anatomy of the ovary, demonstrating hypointense cortex and intermediate to high signal intensity medulla.[18,35,36] The high intensity of the medulla is secondary vascularloose connective tissue. In postmenopausal women, there is decreased signal on T2-weighted images in the medulla due to paucity of follicles and decreased vascular connective tissue.[37,38] Several high signal intensity cysts are identified within the cortex on T2-weighted images. In the premenopausal age group, the normal ovary demonstrates multiple peripherally located follicles, generally measuring less than 3 cm—these are low signal intensity on T1-weighted images and high signal intensity on T2-weighted images with thin enhancing walls.[38] The corpus luteum cyst is an involuting dominant functional cyst and tend to have a more irregular wall. When hemorrhage is present within the corpus luteum cyst, it demonstrates intermediate to high signal intensity on T1-weighted and T2-weighted images depending on the phase of hemorrhage. These cysts demonstrate heterogeneous postgadolinium enhancement in the wall.[36,37]

MALE PELVIS

Technical Considerations

The use of MRI in evaluation of the male genitourinary tract/pelvis is less common due to the inherent differences in internal anatomy. With much of the male genitourinary tract located superficially, ultrasound is the preferred method for cross-sectional imaging of the scrotum and penis; MRI can be a useful problem solving modality for sonographically equivocal or discordant clinical findings.[39,40] A circular/ring-shaped surface coil is preferred, although a short phased-array surface coil can also be used (such as a cardiac coil). The penis is frequently dorsiflexed against the lower midabdomen and taped to reduce motion.[41] Axial, coronal, and sagittal T2-weighted fast spin-echo imaging is performed, using a small FOV, high-resolution matrix, and thin section imaging (Figs. 15A and 16); coronal imaging is often performed using chemical fat-suppression as well. Axial precontrast T1-weighted spin-echo is obtained similar parameters to the T2-weighted imaging sequences. Finally, precontrast and postcontrast sagittal T1-weighted spoiled gradient echo imaging is performed with chemical fat suppression to increase visual detection of subtle enhancement (see Fig. 15B).

Few studies at the authors' institution are specifically ordered for primary evaluation of the male bladder—more frequently, such investigations are performed as part of a magnetic resonance urography study. Additionally, the urinary bladder can typically be well seen on the general female pelvis protocol, which can be modified for the male gender by converting long-axis and short-axis T2-weighted imaging into traditional axial and coronal planes.

There is mounting evidence that imaging patients with a suspected perianal fistula can have substantial benefit, including better initial depiction of fistula geometry, improved triage for surgical management, and superior monitoring for treatment failures.[13,14] At the authors' institution, a high field strength magnet (3.0 Tesla [T]) is used in combination with a surface phased-array coil for perianal imaging; the improved signal at 3.0 T and lack of substantial bowel motion facilitates high spatial resolution imaging of this area. A high-resolution axial T2-weighted fast spin-echo sequence is obtained, using a wide FOV (36 cm) with high 600 $\times$ 800 matrix. Similarly, a high-resolution fat-suppressed sagittal T2-weighted sequence is centered on the perianal region with smaller FOV (20 cm) with a 400 $\times$ 400 matrix providing high spatial detail. Parallel imaging with acceleration factors of 1.5 to 3.0 are used to decrease imaging times. Other lower-resolution, water-sensitive sequences with fat suppression complement these 2 sequences, including short TI inversion recovery (STIR) imaging. High-resolution precontrast and postcontrast axial T1-weighted 3-D spoiled gradient-echo imaging is performed, using small FOV (25 cm), thin 1-mm reconstructed slice thickness,

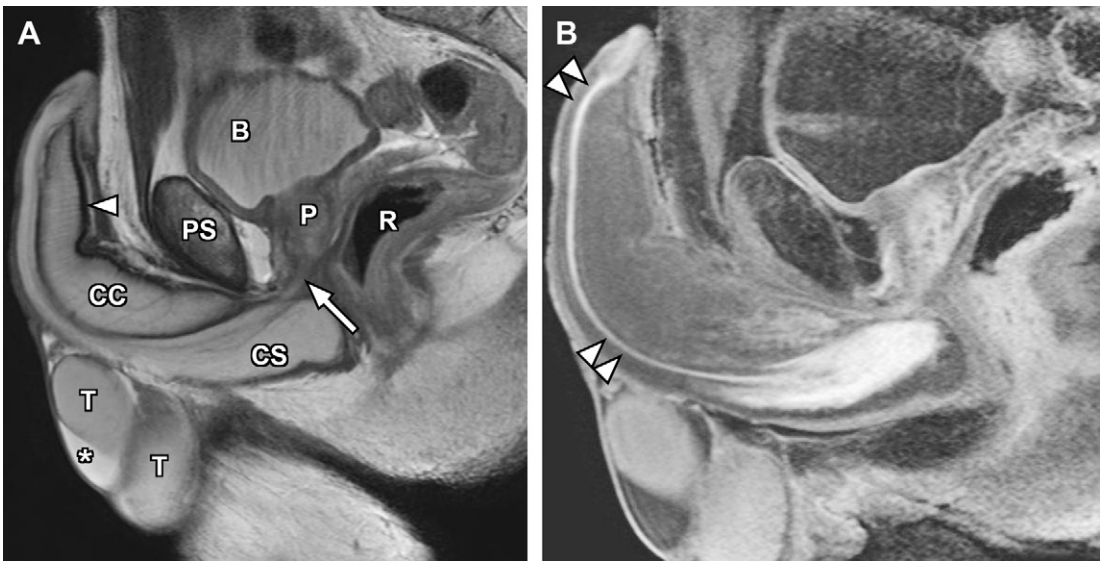

Fig. 15. Midline male pelvis. Sagittal T2-weighted (*A*) and sagittal fat-suppressed postcontrast T1-weighted (*B*) images demonstrate normal penis and scrotal structures. The paired dorsal corpora cavernosa and single ventral corpus spongiosum. Dark surrounding tunica albuginea/fascial layer (*arrowhead*). Testes show homogeneous signal on both T2-weighted images and postcontrast images; note small hydrocele (*asterisk*). Prostate and portion of the posterior urethra (*arrow*) are seen. There is intense mucosal enhancement associated with the urethra on postcontrast imaging (*arrowheads*). B, bladder; CC, corpora cavernosa; CS, corpus spongiosum; P, prostate; PS, pubic symphysis; R, rectum; T, testes.

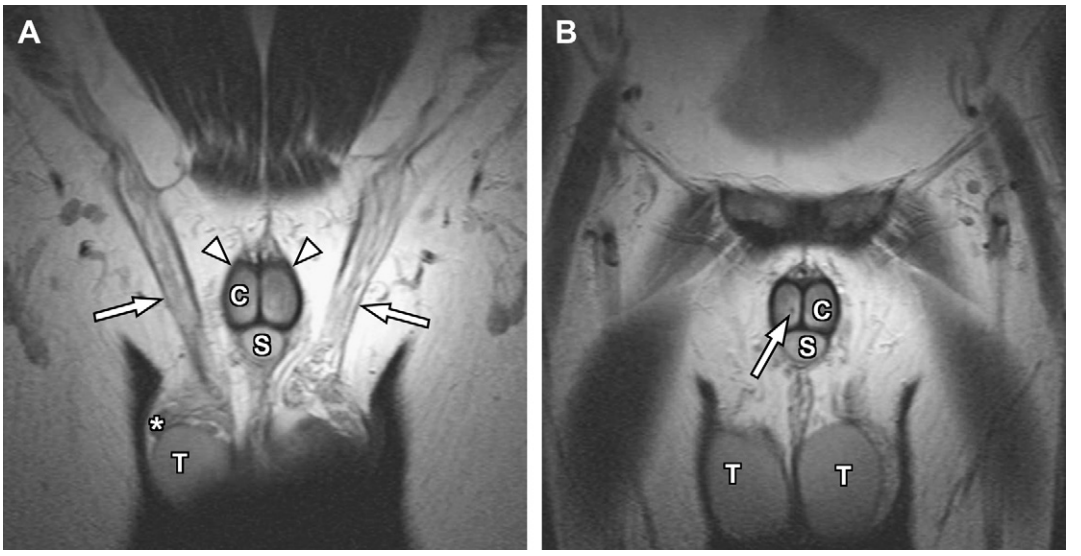

Fig. 16. (*A*) Coronal T2-weighted images through the penis and scrotum, anterior cut. The coronal plane of imaging displays the cross-sectional anatomy of the penis as it approaches the perineum, with right corpus cavernosa and corpus spongiousm marked. Tunica albuginea fascia (*arrowheads*) shows stark hypointensity on T2-weighted images. Spermatic cords (*arrows*) are seen coursing through the inguinal canals. Right testis and epididymis (*asterisk*) are partially visualized. (*B*) Coronal T2-weighted images through the penis and scrotum, middle cut. The testes are now well seen bilaterally, with uniform homogeneous internal signal on T2-weighted images. The right cavernosal artery can be seen as a small flow void (*arrow*) in the right corpus cavernosa. C (*A*), right corpus cavernosa; C (*B*), left corpus cavernosa; S, corpus spongiosum; T, testes.

and a 256 × 512 matrix. Similar high-resolution postcontrast sagittal and coronal planes are also routinely obtained.

Anatomic Considerations and MRI Features

Testes

The testes lie within the scrotal sac, encased by fibrous tunica albuginea that invaginates the testis posteriorly to form mediastinum testis. The processes vaginalis is an extension of the peritoneum into the scrotal sac. The efferent ductules are formed from 400 to 600 seminiferous tubules, which converge in the epididymal head and course through the epididymal body and tail to the vas deferens. The spermatic cord contains vas deferens, testicular artery, venous plexus, and lymphatics as it crosses the inguinal canal. The vas deferens merges with the ejaculatory ducts carrying seminal fluid from the seminal vesicles and opens to the prostatic urethra near the verumontanum.

Even though sonography remains primary modality of choice for evaluation of scrotum and penis, MRI may be used as problem-solving modality in cases where ultrasound is suboptimal or equivocal.[42,43] The testicles are distinctly identified on both T1-weighted and T2-weighted images, enveloped by the tunica albuginea which is low signal intensity on both T1-weighted and T2-weighted images. Normal testes are ovoid structures with homogeneous intermediate signal intensity on T1-weighted images and high signal intensity relative to skeletal muscle on T2-weighted images (see **Figs. 15** and **16**).[44] The mediastinum testis is seen as a low T2 signal intensity band.[41,45] T2-weighted images are best used in evaluation of focal lesion or mass due to better tissue contrast. T1-weighted images are useful in evaluation of hematoma or fat containing tumors. Normally, a small amount of simple fluid is present between the tunica vaginalis, demonstrating high signal on T2-weighted images. The epididymis is isointense to the testis on T1-weighted images and lower in signal intensity on T2-weighted images.[41] The pampiniform plexus lies superior to the epididymal head and may be demonstrated by multiple flow voids depending on flow speeds. When varicoceles are present, dilation and sluggish flow in the pampiniform plexus are expected, resulting in increased high signal on T2-weighted images.

Penis

The penis is comprised of 3 tubular compartments, namely a single ventral corpus spongiosum and paired dorsal corpora cavernosa, enveloped by a thin layer of connective tissue called the tunica albuginea. Peripheral to the tunica albuginea is an additional connective tissue layer, called the Buck fascia, which also serves to separate the dorsal and ventral compartments of the penis.[45,46] The posterior segments of the corpora cavernosa are referred to as the crura and attach to the ischiopubic ramus, becoming contiguous with ischiocavernosus muscle inferiorly. The corpus spongiosum forms the glans penis anteriorly and the penile bulb posteriorly, which is attached to the urogenital diaphragm.[39,41,46] The urethra originates from the bladder base and is generally divided into posterior and anterior segments. The posterior urethra is anatomically divided into 2 subcomponents, namely the prostatic and membranous segments, where the urethra traverses the prostate and urogenital diaphragm, respectively. As the urethra courses from the urogenital diaphragm into the penis itself, it is referred to as the anterior urethra, surrounded by the corpus spongiosum along its entire length and nominally divided into bulbous and pendulous segments. Several of the small vessels supplying the penis can be identified on dedicated small FOV imaging, including the centrally located cavernosal arteries within the substance of the corpora cavernosa, the deep dorsal vein which lies between the tunica albuginea and the Buck fascial layers, and sometimes the paired deep dorsal arteries that run adjacent to the lateral aspects of the deep dorsal vein.

The corpora cavernosa and spongiosa are of intermediate signal intensity on T1-weighted images. On T2-weighted images, the corpus spongiosum demonstrates homogeneous high signal intensity relative to the skeletal muscle (see **Figs. 15** and **16**). The corpora cavernosa may have a heterogeneous signal intensity versus that of the corpus spongiosum, depending on the perfusion distribution. The bulb of the penis demonstrates high signal intensity on T2-weighted images. The tunica albuginea, which surrounds the corpus spongiosum and corpora cavernosa, is of low signal intensity on T1 and T2-weighted images; it can be difficult to separate the tunica lbuginea fascia from the Buck fascia, particularly around the corpora cavernosa, such that the 2 fascia actually form a single thick hypointense rim on T1-weighted and T2-weighted sequences.[39,45,46] The cavernosal arteries are located medially within the corpora cavernosa and are seen as a flow void on T2-weighted images. Postgadolinium images show increased signal intensity of corpora cavernosa, proceeding both from central to peripheral and from proximal to distal, as expected given the location of the cavernosal arteries (see **Fig. 15**B).

Urinary bladder

The bladder is a muscular sac located in the lower pelvis posterior and superior to the pubis. The superior surface of the bladder is covered with peritoneum, which dips down posteriorly and forms the vesicouterine pouch in females and rectovesical pouch in males. From the bladder apex to the umbilicus is a fold of peritoneum, which is remnant of the urachus.

The thickness of bladder wall depends on its distension, varying between 2 and 8 mm.[47] From central to peripheral, the layers of the bladder include the mucosa, submucosa, muscularis containing circular, and longitudinal muscle fibers, and the outer serosa, consisting of adventitious layer. The trigone is the smooth triangular region between the openings of the 2 ureters and urethra and does not feature mucosal folds, even when the bladder is empty.

The bladder receives arterial supply from the internal iliac arteries via superior and inferior vesical arteries. The bladder is also in part supplied by the branches from obturator, uterine, and vaginal arteries. Venous drainage is via a complex plexus draining into the internal iliac vein. Lymphatic drainage is to the common and internal iliac chain.[48,49]

The urine within the bladder appears as low signal on T1-weighted images whereas the bladder wall is also low signal intensity but slightly higher than intraluminal fluid. On T2-weighted images the urine is of high signal intensity and the bladder wall remains of low signal intensity. Bladder mucosa and submucosa may enhance early during dynamic postcontrast T1-weighted images, whereas the muscularis can enhance on delayed imaging.[44] Excreted gadolinium in the bladder has variable signal intensity depending on the concentration of the contrast.[47]

Several normal variants and congenital anomalies of the bladder have been described, including bladder diverticulum, duplication, patent urachus, bladder exstrophy, or agenesis. A bladder diverticulum can be congenital or acquired from chronic outlet obstruction and is usually well depicted on MRI as a focal outpouching from the bladder wall containing urine. Diverticula lead to localized urine stasis, which may result in inflammation, chronic infection, and dysplasia/metaplasia. Incomplete obliteration of the urachus may persist as urachal cyst, sinus, or diverticulum. A ureterocele is a congenital dilation of the submucosal component of distal ureter as it crosses through the urinary bladder wall. Generally, ureteroceles are classified into orthotopic or ectopic in location (**Fig. 17**). Orthotopic ureteroceles can be clinically occult and noted only incidentally on imaging studies. Alternatively, ectopic ureteroceles are often associated with a duplicated collection system, frequently representing the aberrant insertion of an upper pole moiety. In such cases, patients often present clinically with a urinary tract infection, often due to obstruction of the upper tract system.[44]

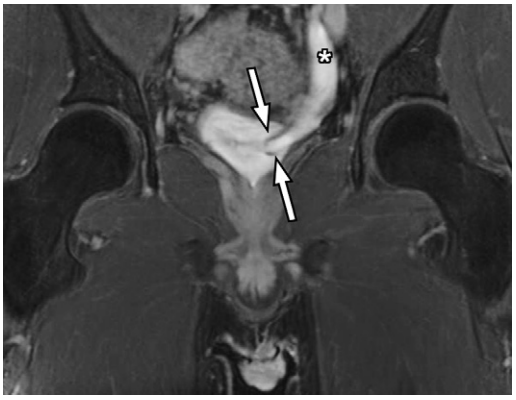

Fig. 17. Incidental left orthotopic ureterocele. Coronal fat suppressed postcontrast T1-weighted image demonstrates bulging intramural segment of the distal left ureter (*arrows*) with some mild upstream collecting system dilation (*asterisk*).

Prostate and seminal vesicles

Technical considerations The role of imaging in the setting of suspected prostatic malignancy has historically been of relatively minor value to treating physicians, most frequently using transrectal ultrasound for guidance during biopsy. Unfortunately, even biopsy can be a misleading standard, with reported false-negative rates of up to 40%.[50] As MRI technology and techniques have advanced, the use of MRI for evaluation of prostate cancer has become more clinically relevant. Local imaging of the prostate by MRI yields images with high spatial and contrast resolution, permitting excellent morphologic depiction of the prostate. Emerging functional techniques, such as diffusion-weighted imaging, MR spectroscopy, and dynamic contrast-enhanced MRI, are areas of active investigation, because these may be useful adjuncts to morphologic imaging.[50,51] At the authors' institution, prostate MRI is performed for local tumor morphologic depiction in the setting of known prostate carcinoma. The standard protocol uses a 1.5-T scanner with an endorectal coil for local imaging and a phased-array surface coil for whole pelvis imaging. The protocol consists of axial, coronal, and sagittal T2-weighted fast spin-echo imaging with small FOV (14 cm) and high resolution (**Figs. 18** and **19**).

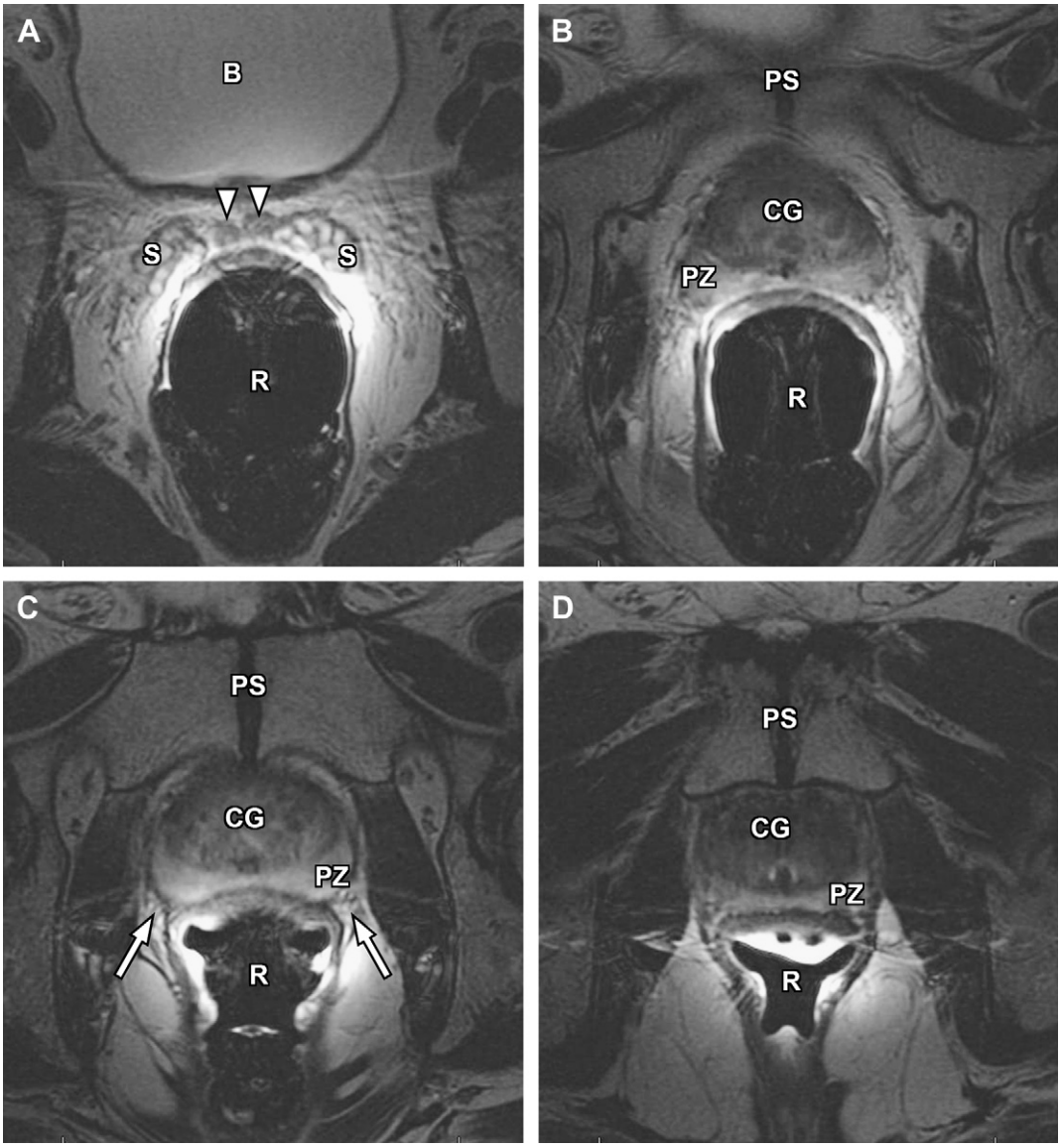

Fig. 18. Small FOV prostate examination with endorectal coil. Axial T2-weighted images from superior to inferior, including above the prostate (*A*), at the prostatic base (*B*), at the midgland (*C*), and at the apex (*D*). Note the zonal anatomy of the prostate, which can include the central gland and peripheral zone following the practical integrated approach. The peripheral zone demonstrates uniform high signal intensity, while the central gland is more heterogeneously low signal. The seminal vesicles and vas deferens (*arrowheads*) are seen toward the superior aspect of the gland. Neurovascular bundles (*arrows*) run in the periprostatic fat at the 5:00 and 7:00 positions relative to the prostate. B, bladder; CG, central gland; PS, pubic symphysis; PZ, peripheral zone; R, rectum with receiver coil; S, seminal vesicles.

Matched axial spin-echo T1-weighted imaging with small FOV, similar to the T2-weighted imaging, is critical for delineating postbiopsy change or hemorrhage. Finally, whole-pelvis imaging is performed using a wide FOV in conjunction with the surface coil. Although prostatic imaging can be performed using a high field strength magnet (3.0 T) with a surface phased-array coil in patients who cannot tolerate endorectal coil placement, published data regarding image quality are conflicting.[52,53] As such, this is considered a secondary option at the authors' institution, with preference given to 1.5-T imaging using an endorectal coil.

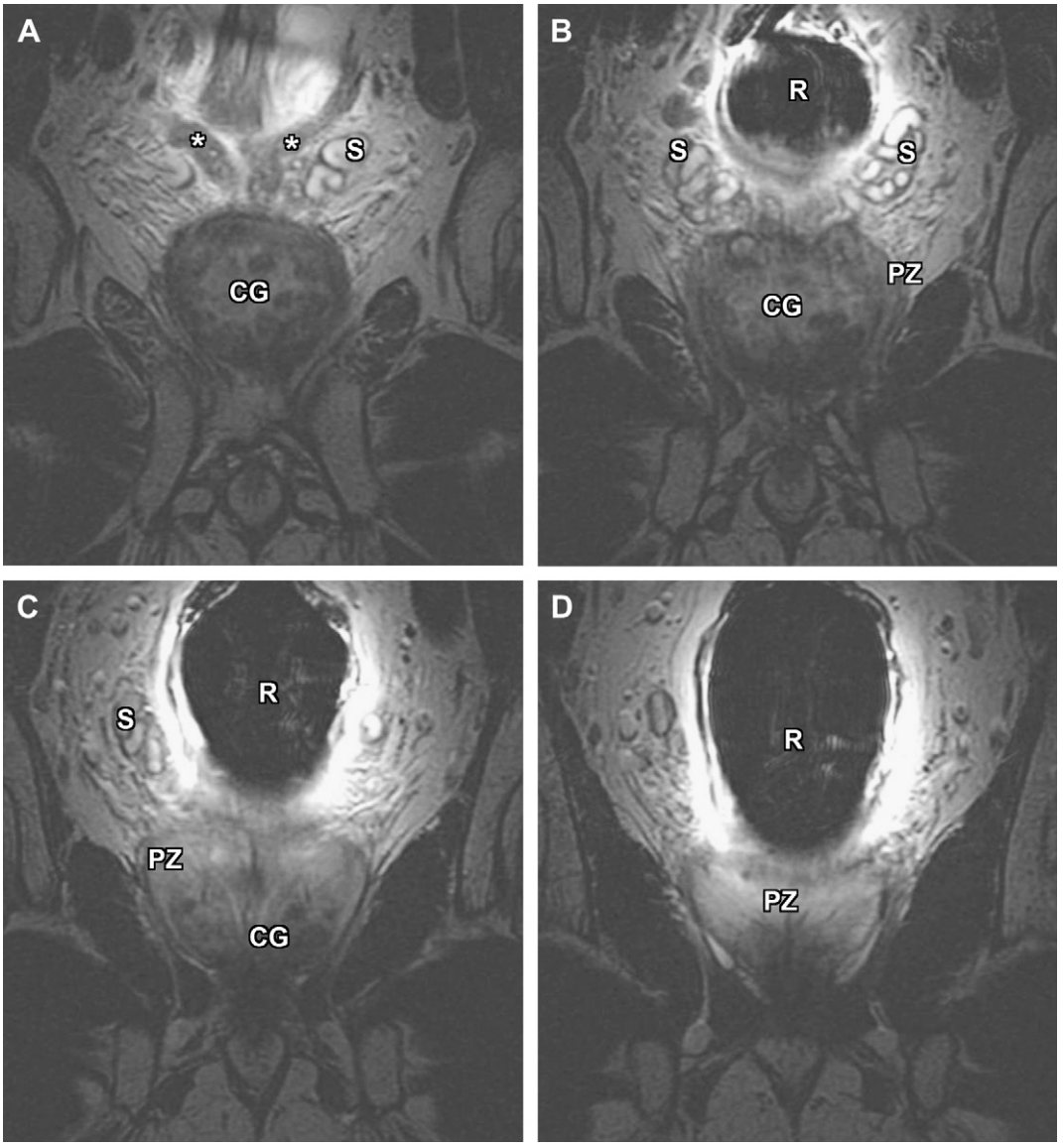

Fig. 19. Small FOV prostate examination with endorectal coil. Coronal T2-weighted images from anterior to posterior (*A–D*). Zonal anatomy of prostate is more difficult to appreciate in the coronal plane, as the transition from central gland to peripheral zone is somewhat subtle given the geometry of the imaging plane. The high signal intensity of the peripheral zone, however, is again conspicuous versus the heterogeneous low signal central gland. Seminal vesicles and vas deferens (*astrisk*) are demonstrated. CG, central gland; PZ, peripheral zone; R, rectum with receiver coil; S, seminal vesicles.

Anatomic considerations and MRI features The prostate is an exocrine gland found only in males and consists of a glandular part (70%) and fibromuscular stroma (30%).[41] It is located just below the urinary bladder and almost equals the size of a walnut. The prostate gland surrounds the proximal urethra (also called prostatic urethra). The ejaculatory ducts coming from the seminal vesicles opens into the prostatic urethra at a site called verumontanum. The seminal vesicle receives sperm from the testicles via vas deferens. The main function of prostate gland is to secrete alkaline fluid that aids in liquefying semen. There are several anatomic classifications of prostatic anatomy, including traditional lobar divisions and a more contemporary zonal classification.[54] The zonal description divides the prostate into glandular and nonglandular elements, the latter of which includes the anterior fibromuscular stroma and the prostatic urethra. The glandular elements can be further

Table 1
Example protocols

Female Pelvis

	Coronal T2 Wide FOV	Sagittal T2	Long-Axis T2	Short-Axis T2	Axial In/ Opposed T1	Axial Pre-/ Post-T1 FS
Pulse Sequence	SSFSE	FSE	FSE	FSE	SPGR	SPGR, FS
Repetition Time (ms)	Minimum	3000–4000	3000–4500	3000–4500	205	190
Echo Time (ms)	180	96	96	96	2.3/4.6	Minimum
FOV (cm)	40	24–32	20–24	20–24	28–34	24–32
Slice Thickness (mm)	8	5	5	5	6	6
Matrix	256 × 128	512 × 224	512 × 224	512 × 224	256 × 160	320 × 160
Signal Averages	0.5	4	4	4	1	1

Female Urethra

	Axial Small FOV	Sagittal Small FOV	Axial Pre-/Post-T1 FS
Pulse Sequence	FSE	FSE	SE, FS
Repetition Time (ms)	4200	3000	450
Echo Time (ms)	85	85	Minimum
FOV (cm)	18	20	18
Slice Thickness (mm)	4	5	4
Matrix	512 × 224	256 × 224	256 × 224
Signal Averages	4	4	2

Male Penis/Scrotum

	Coronal T2 Wide FOV	Axial T1	Axial T2	Sagittal T2	Sagittal Pre-/Post-T1 FS
Pulse Sequence	SSFSE	SE	FSE	FSE	SPGR, FS
Repetition Time (ms)	Minimum	650	4200	3000	220
Echo Time (ms)	90	Minimum	85	85	Minimum
FOV (cm)	30	18	18	20	20
Slice Thickness (mm)	6	4	4	5	6
Matrix	256 × 128	256 × 224	256 × 224	256 × 224	512 × 160
Signal Averages	0.5	2	4	4	2

Fistula

	Axial T2 HR	Sagittal T2 FS	Axial Pre-/Post-T1 HR FS
Pulse Sequence	TSE	SE	3-D FFE
Repetition Time (ms)	Minimum	Minimum	Minimum
Echo Time (ms)	80	80	Minimum
FOV (cm)	36	20	25
Slice Thickness (mm)	6	6	1
Matrix	800 × 600	400 × 400	512 × 256
Signal Averages	4	4	8

Prostate

	Axial T2	Coronal T2	Sagittal T2	Axial T1	Axial T1 Whole Pelvis
Pulse Sequence	FSE	FSE	FSE	SE	SE
Repetition Time (ms)	5100	5000	5000	675	700
Echo Time (ms)	120	120	120	Minimum	Minimum
FOV (cm)	14	14	14	14	38
Slice Thickness (mm)	3	3	3	3	6
Matrix	256 × 192	256 × 192	256 × 192	256 × 160	256 × 192
Signal Averages	4	4	4	2	2

Abbreviations: FFE, fast field echo; FOV, field of view; FS, fat saturation; FSE, fast spin echo; HR, high resolution; SE, spin echo; SPGR, spoiled gradient recalled echo; SSFSE, single shot fast spin echo; TSE, turbo spin echo.

divided into inner and outer components. Subdivisions of the inner component include the periurethral tissue and the transition zone, whereas the outer components can be divided into the smaller central zone and the larger peripheral zone. The transitional zone comprises 5% of the prostate volume in young adults and surrounds the anterior-lateral aspect of the proximal urethra in a curvilinear fashion. The central zone constitutes 25% of the prostate volume in young adults and abuts the posterior-superior aspect of the proximal urethra.[45] The volumetric contribution of the transitional zone and central zone change with age, because the transitional zone is primarily involved by benign prostatic hyperplasia, leading to growth and compression of the central zone in older.[54] The peripheral zone accounts for 70% of the volume of the prostate and contains most of the glandular tissue; 70% of the prostate cancer originates in the peripheral zone, 20% in transitional zone, and 10% in central zone.[41,45,55,56] The zonal classification is often modified for radiologic use, where the term, *central gland*, collectively refers to the periurethral tissues, transitional zone, and the central zone. The peripheral zone is, therefore, referenced independently of the central gland, often in the practical integrated approach to prostatic anatomy.[45,54] Some investigators group the central zone and peripheral zone together as the peripheral gland, although this subtle nomenclature difference can confuse readers versus the practical integrated approach and is not used in this article.

On T1-weighted image, the normal prostate has relatively homogeneous low to intermediate signal intensity with poor differentiation of zonal anatomy.[45] The zonal anatomy is better defined on T2-weighted sequence. On T2-weighted images, the prostatic signal intensity depends on the proportion of glandular tissue versus stromal or muscular components, with glandular tissue normally demonstrating high signal intensity whereas fibromuscular stromal elements have low signal intensity. Thus, the normal peripheral zone is relatively high signal intensity due to presence of rich glandular tissue whereas the central and transitional zones are more hypointense due to increased stromal components. The central gland is separate from the peripheral zone by a low T2 signal intensity band of tissue known as the surgical capsule. The true prostate capsule is comprised of fibromuscular tissue that is of low signal intensity on T2-weighted image and separates the high signal intensity peripheral zone of the prostate from the periprostatic soft tissues.[41,45]

The neurovascular bundles are located posterolaterally within the rectoprostatic region at the 5:00 and 7:00 positions and include the nerves innervating the corpora cavernosa and venous plexuses. These bundles are of low signal intensity relative to the surrounding periprostatic fat (see **Fig. 18**C).

The seminal vesicles are paired structure located above the prostate. Each seminal vesicle is composed of multiple lobules containing high T2 signal intensity simple fluid with hypointense wall, giving a cluster of grapes appearance.[41,45] After 60 years of age, the fluid content in the seminal vesicles may decrease symmetrically, thereby causing lower signal intensity on T2WI.[45]

SUMMARY

The superior tissue contrast and flexible imaging planes afforded by MRI versus competing technologies permits optimal depiction of the pelvic viscera. Targeted protocols developed for specific pelvic visceral organs highlight important anatomic features that may not be imaged by other modalities (**Table 1**). Therefore, a solid understanding of normal and variant pelvic anatomy is crucial for appropriate interpretation of pelvic MRI studies.

REFERENCES

1. Rezvani M, Shaaban A. Imaging of cervical pathology. Clin Obstet Gynecol 2009;52(1):94–111.
2. Jeong YY, Outwater EK, Kang HK. Imaging evaluation of ovarian masses. Radiographics 2000;20(5): 1445–70.
3. Imaoka I, Wada A, Kaji Y, et al. Developing an MR imaging strategy for diagnosis of ovarian masses. Radiographics 2006;26(5):1431–48.
4. Troiano RN, McCarthy SM. Mullerian duct anomalies: imaging and clinical issues. Radiology 2004; 233(1):19–34.
5. Kroencke TJ, Scheurig C, Kluner C, et al. Uterine fibroids: contrast-enhanced MR angiography to predict ovarian artery supply—initial experience. Radiology 2006;241(1):181–9.
6. Chou CP, Levenson RB, Elsayes KM, et al. Imaging of female urethral diverticulum: an update. Radiographics 2008;28(7):1917–30.
7. Chaudhry S, Reinhold C, Guermazi A, et al. Benign and malignant diseases of the endometrium. Top Magn Reson Imaging 2003;14(4):339–57.
8. Nalaboff KM, Pellerito JS, Ben-Levi E. Imaging the endometrium: disease and normal variants. Radiographics 2001;21(6):1409–24.
9. McCarthy S, Tauber C, Gore J. Female pelvic anatomy: MR assessment of variations during the menstrual cycle and with use of oral contraceptives. Radiology 1986;160(1):119–23.

10. Brown HK, Stoll BS, Nicosia SV, et al. Uterine junctional zone: correlation between histologic findings and MR imaging. Radiology 1991;179(2):409–13.
11. McCarthy S, Scott G, Majumdar S, et al. Uterine junctional zone: MR study of water content and relaxation properties. Radiology 1989;171(1):241–3.
12. Scoutt LM, Flynn SD, Luthringer DJ, et al. Junctional zone of the uterus: correlation of MR imaging and histologic examination of hysterectomy specimens. Radiology 1991;179(2):403–7.
13. Reinhold C, McCarthy S, Bret PM, et al. Diffuse adenomyosis: comparison of endovaginal US and MR imaging with histopathologic correlation. Radiology 1996;199(1):151–8.
14. Lee JK, Gersell DJ, Balfe DM, et al. The uterus: in vitro MR-anatomic correlation of normal and abnormal specimens. Radiology 1985;157(1):175–9.
15. Hricak H, Alpers C, Crooks LE, et al. Magnetic resonance imaging of the female pelvis: initial experience. AJR Am J Roentgenol 1983;141(6):1119–28.
16. Brown MA, Kubik-huch RA, Reinhold C, et al. Uterus and cervix. In: Semelka RC, editor. 2nd edition, Abdominal pelvic MRI, vol. 1. New Jersey: John Wiley & Sons, Inc; 2006. p. 1251–332.
17. Scoutt LM, McCauley TR, Flynn SD, et al. Zonal anatomy of the cervix: correlation of MR imaging and histologic examination of hysterectomy specimens. Radiology 1993;186(1):159–62.
18. Siegelman ES. MRI of the female pelvis. In: Siegelman ES, editor. Body MRI. 1st edition. Philadelphia: Elsevier Saunders; 2005. p. 269–342.
19. deSouza NM, Hawley IC, Schwieso JE, et al. The uterine cervix on in vitro and in vivo MR images: a study of zonal anatomy and vascularity using an enveloping cervical coil. AJR Am J Roentgenol 1994;163(3):607–12.
20. The American Fertility Society classifications of adnexal adhesions, distal tubal occlusion, tubal occlusion secondary to tubal ligation, tubal pregnancies, mullerian anomalies and intrauterine adhesions. Fertil Steril 1988;49(6):944–55.
21. Ascher SM, Scoutt LM, McCarthy SM, et al. Uterine changes after dilation and curettage: MR imaging findings. Radiology 1991;180(2):433–5.
22. Togashi K, Kawakami S, Kimura I, et al. Uterine contractions: possible diagnostic pitfall at MR imaging. J Magn Reson Imaging 1993;3(6):889–93.
23. Togashi K, Kawakami S, Kimura I, et al. Sustained uterine contractions: a cause of hypointense myometrial bulging. Radiology 1993;187(3):707–10.
24. Woo GM, Twickler DM, Stettler RW, et al. The pelvis after cesarean section and vaginal delivery: normal MR findings. AJR Am J Roentgenol 1993;161(6):1249–52.
25. Hricak H, Chang YC, Thurnher S. Vagina: evaluation with MR imaging. Part I. Normal anatomy and congenital anomalies. Radiology 1988;169(1):169–74.
26. Eisenberg LB, Semelka RC, Firat Z. Female urethra and vagina. In: Semelka RC, editor. Abdominal pelvic MRI. 2nd edition. New Jersey: John Wiley & Sons. Inc; 2006. p. 1219–49.
27. Siegelman ES, Outwater EK, Banner MP, et al. High-resolution MR imaging of the vagina. Radiographics 1997;17(5):1183–203.
28. Griffin N, Grant LA, Sala E. Magnetic resonance imaging of vaginal and vulval pathology. Eur Radiol 2008;18(6):1269–80.
29. Preidler KW, Tamussino K, Szolar DM, et al. Staging of cervical carcinomas. Comparison of body-coil magnetic resonance imaging and endorectal surface coil magnetic resonance imaging with histopathologic correlation. Invest Radiol 1996;31(7):458–62.
30. Nurenberg P, Zimmern PE. Role of MR imaging with transrectal coil in the evaluation of complex urethral abnormalities. AJR Am J Roentgenol 1997;169(5):1335–8.
31. Siegelman ES, Banner MP, Ramchandani P, et al. Multicoil MR imaging of symptomatic female urethral and periurethral disease. Radiographics 1997;17(2):349–65.
32. Hricak H, Secaf E, Buckley DW, et al. Female urethra: MR imaging. Radiology 1991;178(2):527–35.
33. Kim JK, Kim YJ, Choo MS, et al. The urethra and its supporting structures in women with stress urinary incontinence: MR imaging using an endovaginal coil. AJR Am J Roentgenol 2003;180(4):1037–44.
34. Brown MA, Ascher SM, Semelka RC. Adnexa. In: Semelka RC, editor. Abdominal pelvic MRI. 2nd edition. New Jersey: John Wiley & Sons, Inc; 2006. p. 1333–82.
35. Togashi K. MR imaging of the ovaries: normal appearance and benign disease. Radiol Clin North Am 2003;41(4):799–811.
36. Outwater EK, Mitchell DG. Normal ovaries and functional cysts: MR appearance. Radiology 1996;198(2):397–402.
37. Outwater EK, Talerman A, Dunton C. Normal adnexa uteri specimens: anatomic basis of MR imaging features. Radiology 1996;201(3):751–5.
38. Sala EJ, Atri M. Magnetic resonance imaging of benign adnexal disease. Top Magn Reson Imaging 2003;14(4):305–27.
39. Pretorius ES, Siegelman ES, Ramchandani P, et al. MR imaging of the penis. Radiographics 2001;21(Spec No):S283–98 [discussion: S298–9].
40. Muglia V, Tucci S Jr, Elias J Jr, et al. Magnetic resonance imaging of scrotal diseases: when it makes the difference. Urology 2002;59(3):419–23.
41. Pretorius ES, Siegelman ES. MRI of the male pelvis and the bladder. Body MRI. 1st edition. Philadelphia: Elsevier Saunders; 2005. p. 371–424.
42. Woodward PJ, Schwab CM, Sesterhenn IA. From the archives of the AFIP: extratesticular scrotal

masses: radiologic-pathologic correlation. Radiographics 2003;23(1):215–40.
43. Patel MD, Silva AC. MRI of an adenomatoid tumor of the tunica albuginea. AJR Am J Roentgenol 2004; 182(2):415–7.
44. Sica GT, Teeger S. MR imaging of scrotal, testicular, and penile diseases. Magn Reson Imaging Clin N Am 1996;4(3):545–63.
45. Noone TC, Semelka RC, Firat Z, et al. Male pelvis. In: Semelka RC, editor. Abdominal pelvic MRI. 2nd edition. New Jersey: John Wiley & Sons, Inc; 2006. p. 1179–217.
46. Hricak H, Marotti M, Gilbert TJ, et al. Normal penile anatomy and abnormal penile conditions: evaluation with MR imaging. Radiology 1988;169(3): 683–90.
47. Duerdulian C, Firat Z, Brown ED, et al. Bladder. In: Semelka RC, editor. Abdominal-pelvic MRI. 2nd edition. New Jersey: John Wiley & Sons, Inc; 2006. p. 1141–78.
48. Banson ML. Normal MR anatomy and techniques for imaging of the male pelvis. Magn Reson Imaging Clin N Am 1996;4(3):481–96.
49. Teeger S, Sica GT. MR imaging of bladder diseases. Magn Reson Imaging Clin N Am 1996;4(3):565–81.
50. Turkbey B, Albert PS, Kurdziel K, et al. Imaging localized prostate cancer: current approaches and new developments. AJR Am J Roentgenol 2009; 192(6):1471–80.
51. Coakley FV, Qayyum A, Kurhanewicz J. Magnetic resonance imaging and spectroscopic imaging of prostate cancer. J Urol 2003;170(6 Pt 2):S69–75 [discussion: S75–6].
52. Beyersdorff D, Taymoorian K, Knosel T, et al. MRI of prostate cancer at 1.5 and 3.0 T: comparison of image quality in tumor detection and staging. AJR Am J Roentgenol 2005;185(5):1214–20.
53. Sosna J, Pedrosa I, Dewolf WC, et al. MR imaging of the prostate at 3 Tesla: comparison of an external phased-array coil to imaging with an endorectal coil at 1.5 Tesla. Acad Radiol 2004;11(8):857–62.
54. Coakley FV, Hricak H. Radiologic anatomy of the prostate gland: a clinical approach. Radiol Clin North Am 2000;38(1):15–30.
55. Choi YJ, Kim JK, Kim N, et al. Functional MR imaging of prostate cancer. Radiographics 2007; 27(1):63–75 [discussion: 75–7].
56. Hricak H, Dooms GC, McNeal JE, et al. MR imaging of the prostate gland: normal anatomy. AJR Am J Roentgenol 1987;148(1):51–8.